Journal of Rock Mechanics and Geotechnical Engineering 12 (2020) 310–325

Contents lists available at ScienceDirect

Journal of Rock Mechanics and Geotechnical Engineering

journal homepage: www.jrmge.cn

Full Length Article

# GPGPU-parallelised hybrid finite-discrete element modelling of rock chipping and fragmentation process in mechanical cutting

Mojtaba Mohammadnejad [a,b], Sevda Dehkhoda [b,c,**], Daisuke Fukuda [a,d], Hongyuan Liu [a,*], Andrew Chan [a]

[a] School of Engineering, College of Science and Engineering, University of Tasmania, Hobart, TAS, 7001, Australia
[b] CSIRO, Minerals Resources Business Unit, QCAT 1 Technology Court, Pullenvale, QLD, 4069, Australia
[c] Hatch, Brisbane, QLD, 4000, Australia
[d] Division of Sustainable Resources Engineering, Faculty of Engineering, Hokkaido University, Hokkaido, Japan

ARTICLE INFO

*Article history:*
Received 22 March 2019
Received in revised form
13 September 2019
Accepted 9 December 2019
Available online 7 February 2020

*Keywords:*
Numerical simulation
Finite-discrete element method (FDEM)
Rock cutting
Chipping
Cracking

ABSTRACT

Mechanical cutting provides one of the most flexible and environmentally friendly excavation methods. It has attracted numerous efforts to model the rock chipping and fragmentation process, especially using the explicit finite element method (FEM) and bonded particle model (BPM), in order to improve cutting efficiency. This study investigates the application of a general-purpose graphic-processing-unit parallelised hybrid finite-discrete element method (FDEM) which enjoys the advantages of both explicit FEM and BPM, in modelling the rock chipping and fragmentation process in the rock scratch test of mechanical rock cutting. The input parameters of FDEM are determined through a calibration procedure of modelling conventional Brazilian tensile and uniaxial compressive tests of limestone. A series of scratch tests with various cutting velocities, cutter rake angles and cutting depths is then modelled using FDEM with calibrated input parameters. A few cycles of cutter/rock interactions, including their engagement and detachment process, are modelled for each case, which is conducted for the first time to the best knowledge of the authors, thanks to the general purpose graphic processing units (GPGPU) parallelisation. The failure mechanism, cutting force, chipping morphology and effect of various factors on them are discussed on the basis of the modelled results. Finally, it is concluded that GPGPU-parallelised FDEM provides a powerful tool to further study rock cutting and improve cutting efficiencies since it can explicitly capture different fracture mechanisms contributing to the rock chipping as well as chip formation and the separation process in mechanical cutting. Moreover, it is concluded that chipping is mostly owed to the mix-mode I-II fracture in all cases although mode II cracks and mode I cracks are the dominant failures in rock cutting with shallow and deep cutting depths, respectively. The chip morphology is found to be a function of cutter velocity, cutting depth and cutter rake angle.


## 1. Introduction

Over the last decades, application of mechanical tools in rock fragmentation has been extended widely in mining and civil engineering industries since mechanical excavation provides a more flexible and environmentally friendly alternative to conventional blasting, especially in urban or non-ventilated environments. Typically, there are two types of rock cutting processes based on the moving direction of the mechanical tool with respect to the rock surface, i.e. drag bits (or fixed point cutters) and indenters. While a drag bit hits the rock in a direction parallel to the rock surface, an indenter penetrates into the rock surface normally (Hood and Alehossein, 2000). Advances in mechanical cutting tool manufacturing technology, particularly the introduction of high wear-resistance materials, have made mechanical rock cutting with the drag bit an attractive research choice. However, the rock fragmentation mechanism with the mechanical cutter has not been well understood due to the complexity of the interaction between the mechanical tool and rock, and the complex rock fracture

* Corresponding author.
** Corresponding author. Hatch, Brisbane, QLD, 4000, Australia.
*E-mail addresses:* sevda.dehkhoda@hatch.com (S. Dehkhoda), hong.liu@utas.edu.au (H. Liu).
Peer review under responsibility of Institute of Rock and Soil Mechanics, Chinese Academy of Sciences.

https://doi.org/10.1016/j.jrmge.2019.12.004

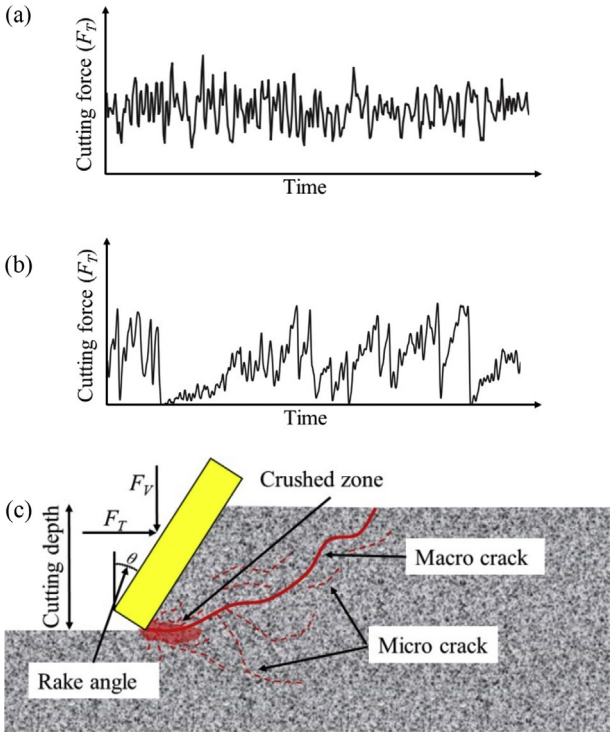


**Fig. 1.** Schematic illustration of chipping mechanism (redrawn after Richard et al., 2012): (a) Cutting force vs. time history under ductile mode of failure; (b) Cutting force vs. time history under brittle mode of failure; and (c) Rock chipping process.

process (Che et al., 2016). While rock cutting experiments are largely used to investigate the cutting process and the associated cutting forces, the extensive number of variables and the effective factors influencing the process have made the application of these

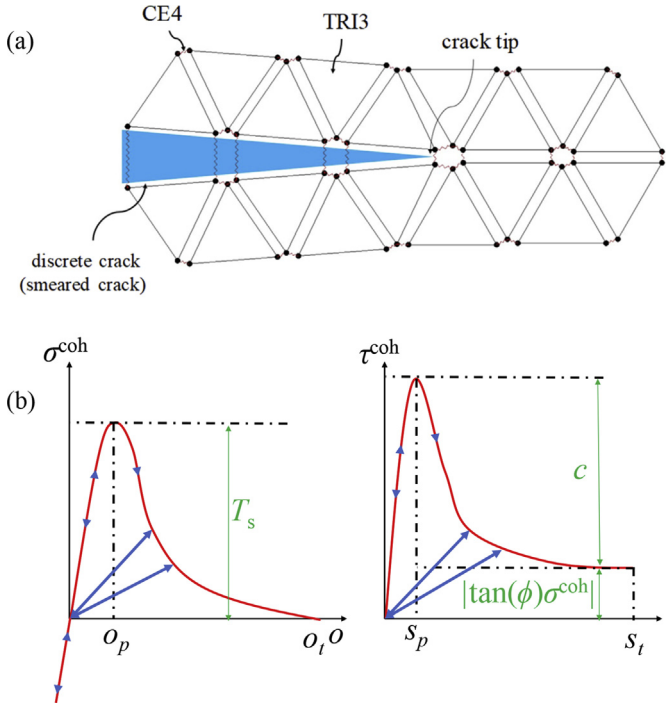


**Fig. 2.** Transition from continuum to discontinuum in 2D Y-HFDEM IDE: (a) Assembly of TRI3s and CE4s, and (b) Tensile/shear softening curves.

**Table 1**
Physical–mechanical properties of rock and numerical parameters.

| Parameter | Unit | Value |
|---|---|---|
| Density ($\rho$) | kg/m$^3$ | 1800 |
| Young's modulus ($E$) | GPa | 12.2 |
| Poisson's ratio ($\nu$) | – | 0.22 |
| Tensile strength ($T_s$) | MPa | 1.77 |
| Cohesion ($c$) | MPa | 5 |
| Internal friction angle of intact rock ($\phi$) | ° | 25 |
| Mode I fracture energy ($G_{fI}$) | J/m$^2$ | 16 |
| Mode II fracture energy ($G_{fII}$) | J/m$^2$ | 160 |
| Normal contact penalty number ($P_{n\_con}$) | GPa | 1220 |
| Tangent contact penalty number ($P_{tan\_con}$) | GPa/m | 1220 |
| Artificial stiffness penalty ($P_f$, $P_{tan}$, $P_{overlap}$) | GPa/m | 12,200 |
| Average element size ($h_{ave}$) | mm | 0.7 |

experiments relatively limited. Meanwhile, analytical and empirical methods (Detournay and Defourny, 1992; Detournay and Atkinson, 2000) developed so far suffer from many simplistic assumptions. Recent advances in numerical modelling methods have confirmed that numerical methods provide robust tools for simulation of the complex mechanisms such as mechanical rock cutting. Hence, different numerical techniques have been considered for investigation of the rock fracture process due to rock cutting. However, not all of the numerical techniques are able to model the entire rock cutting process. This paper aims to investigate the rock cutting process in scratch tests using a new implementation of the combined finite-discrete element method (FDEM) based on parallel computation using general purpose graphic processing units (GPGPU) which is capable of simulating the full rock cutting process.

This paper is organized as follows. Firstly, an introduction to the rock cutting mechanism is given and its numerical modelling process, as reported in the literature, is reviewed. Then, the GPGPU-based hybrid FDEM and its calibration against the Brazilian tensile strength (BTS) and uniaxial compressive strength (UCS) tests, usually conducted in rock mechanics laboratory for studying rock failure mechanisms, are explained. The chipping and fragmentation process of a rock under the action of a cutter in a rock scratch test is modelled using the calibrated hybrid FDEM. A series of parametric

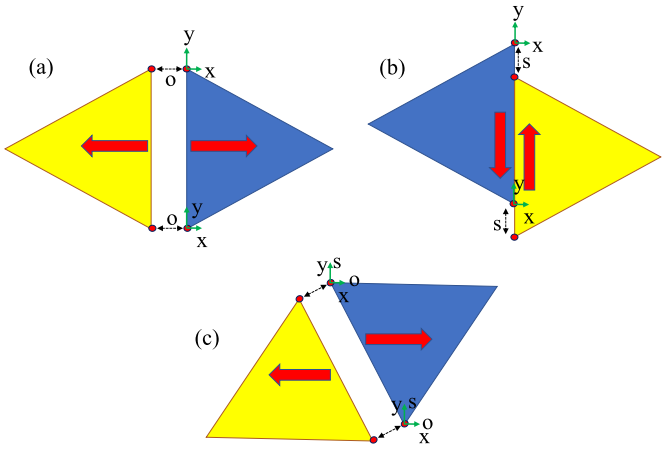


**Fig. 3.** Relationship between local mesh alignment and loading directions: (a) Schematic sketch of the pure mode I fracturing mechanism in a structured mesh with local mesh aligning with tensile loading direction; (b) Schematic sketch of the pure mode II fracturing mechanism in a structured mesh with local mesh aligning with shear loading direction; and (c) Schematic sketch of the mixed mode fracturing mechanism in an unstructured mesh.

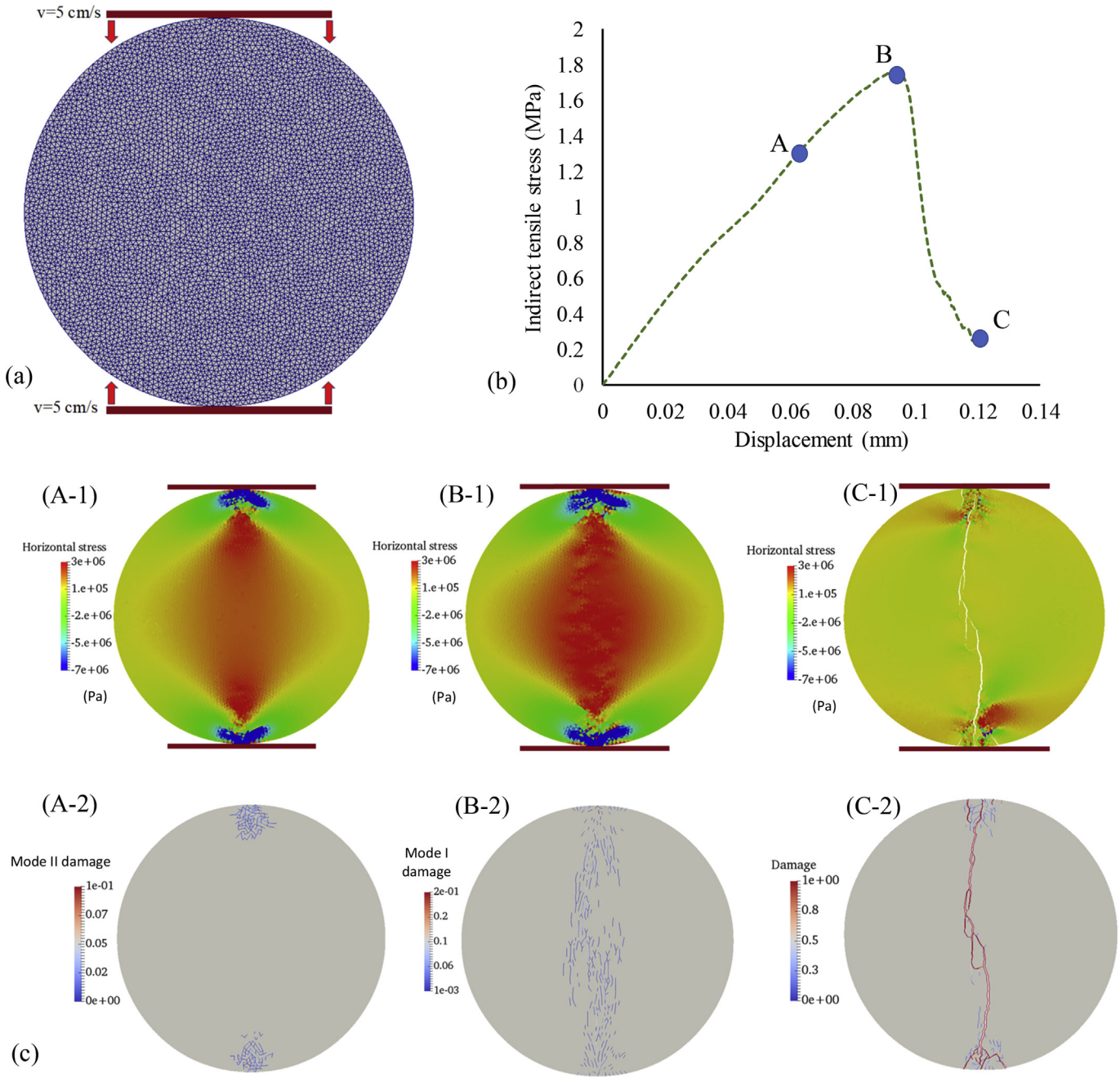


**Fig. 4.** Numerical simulation of Brazilian test: (a) Model geometry; (b) Indirect tensile stress versus axial strain; and (c) Rock failure processes in terms of horizontal stress distribution and damage variable: (A) Extension of shear (mode II) micro-cracks (no macro-cracks) before the peak stress; (B) Tensile (mode I) micro-cracks (no macro-cracks) at the peak stress; and (C) Mixed mode I-II micro- and macro-cracks during the post failure.

studies is carried out to investigate the effect of the important parameters in the mechanical cutting such as back rake angle, cutting speed and cutting depth on the rock cutting process.

## 2. Review on rock chipping mechanism in mechanical cutting and its numerical modelling

### 2.1. Rock failure mechanism in mechanical cutting

Understanding the rock cutting mechanism is a prerequisite for developing efficient cutting technologies. Significant experimental, analytical and numerical studies have been carried out to understand the mechanism of rock cutting under the action of the drag picks. Most of these efforts have been dedicated to improving the efficiency of the rock cutting process and understanding the governing parameters of the rock fracture process. In many cases, the scratch test has been used to investigate the rock cutting process and the mechanics of rock–tool interaction (Richard et al., 2012). Ductile and brittle failure modes are observed in the scratch tests, and their occurrences are suggested to be controlled by rock stiffness (Miedema, 2014) and cutting depth ($d$) (Richard et al., 2012). The ductile (or grinding) mode of failure occurs due to shearing at a shallow cutting depth and the monitored signal of the corresponding cutting force is similar to a white noise (Fig. 1a). By increasing the depth of cutting, the failure mode tends to become a brittle one, also known as the chipping mode. The depth at which

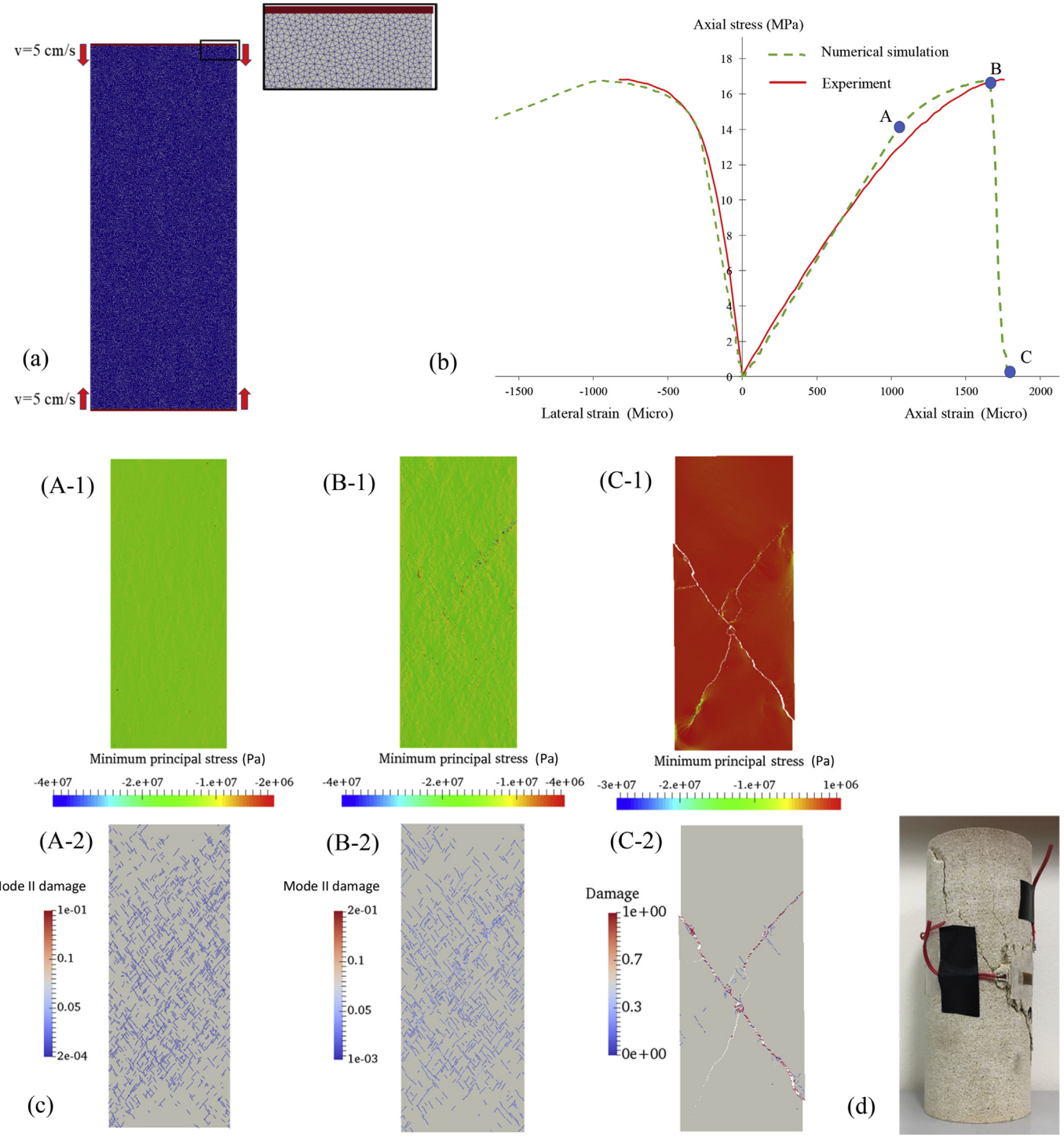


**Fig. 5.** Numerical simulations of UCS test: (a) Model geometry; (b) Axial stress versus axial strain; and (c) Rock failure processes in terms of minimum principal stress distribution and damage variable: (A) Shear (mode II) micro-cracks (no macro-cracks) before the peak stress; (B) Shear (model II) micro-cracks (no macro-cracks) at the peak stress; and (C) Mixed mode I-II micro- and macro-cracks during the post failure; and (d) Final failure pattern observed in the test.

the shearing failure mode starts to turn into the chipping mode is known as critical depth (Richard, 1999). At the critical depth, there is a so-called transition zone, in which transition from shearing to brittle failure takes place.

A number of experimental, theoretical and numerical attempts have been made to determine the critical depth or define correlations between the critical depth and strength parameters of rock in the rock cutting process (Richard, 1999; Huang and Detournay, 2008; He and Xu, 2016; He et al., 2017). Based on the laboratory observations (Richard, 1999), the critical depth for the transition of failure modes in sedimentary rock was in the order of 1 mm. The critical depth ($d^*$) could be defined as a function of mode I fracture toughness ($K_{Ic}$) and rock strength ($q$), i.e. $d^* \propto (K_{Ic}/q)^2$. It has also been shown that there is a good correlation between the cutting force and UCS of the rock for shallow depth cutting in sedimentary rocks (Richard, 1999). Huang and Detournay (2008) introduced the

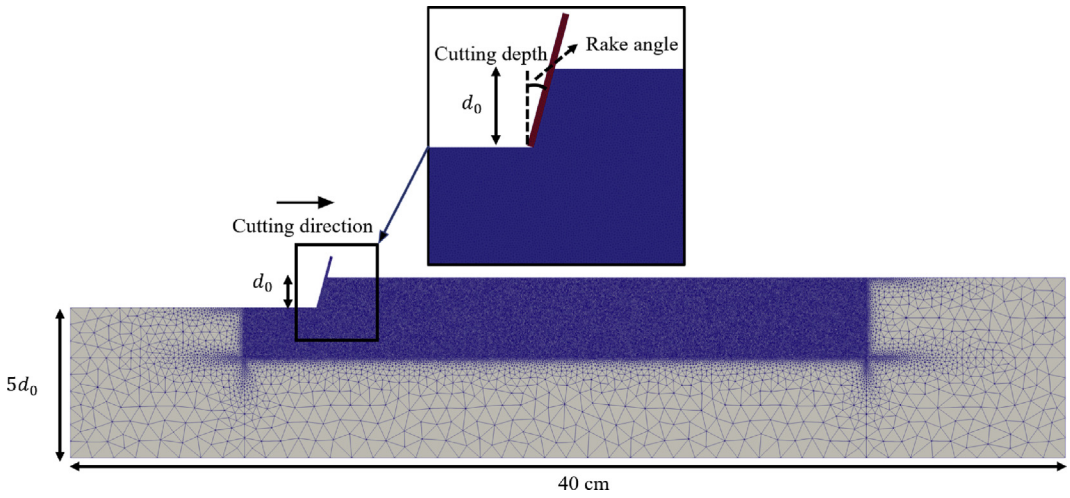


**Fig. 6.** Numerical model of the scratch tests with various cutting velocities, cutter back rake angles and cutting depths.

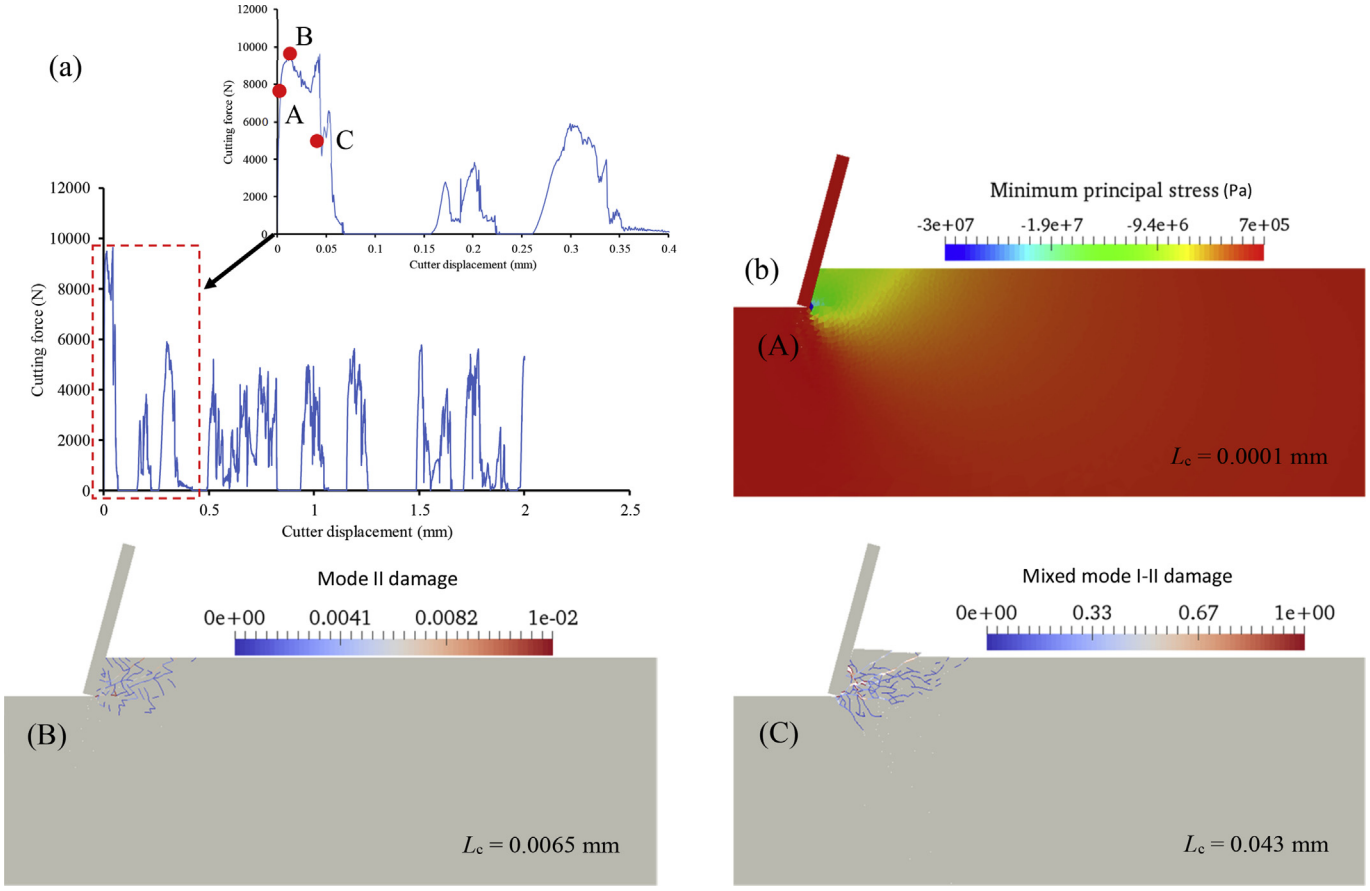


**Fig. 7.** Numerical simulation of the scratch test: (a) Cutting force-cutter displacement history; and (b) Snapshots of the first chipping process: (A) Stress field build-up; (B) Mode II crack initiation and propagation; and (C) Chipping due to mixed mode I-II fracturing.

concept of intrinsic length, $l_m=(1/\pi)(K_{Ic}/\sigma_c)^2$ where $\sigma_c$ is the UCS of the rock, and stated that the critical depth was proportional to $l_m$. Taking into account this study and using Bažant's simple size effect equation (Bazant and Planas, 1997), Zhou and Lin (2013) proposed that the critical depth could be estimated as a proportional function of $\sigma_c$, i.e. $d^* = 5.6{\sigma_c}^{-0.43}$ based on the results from their numerical simulations. He and Xu (2015) numerically showed that the critical transition depth decreased with an increase in the rock brittleness.

A brittle cutting model generally involves rock fracture and chipping. A typical signal of the cutting force shows a saw-tooth pattern (Fig. 1b), due to the continuous forming and detachment of chip segments from the cutting tool. The process can be

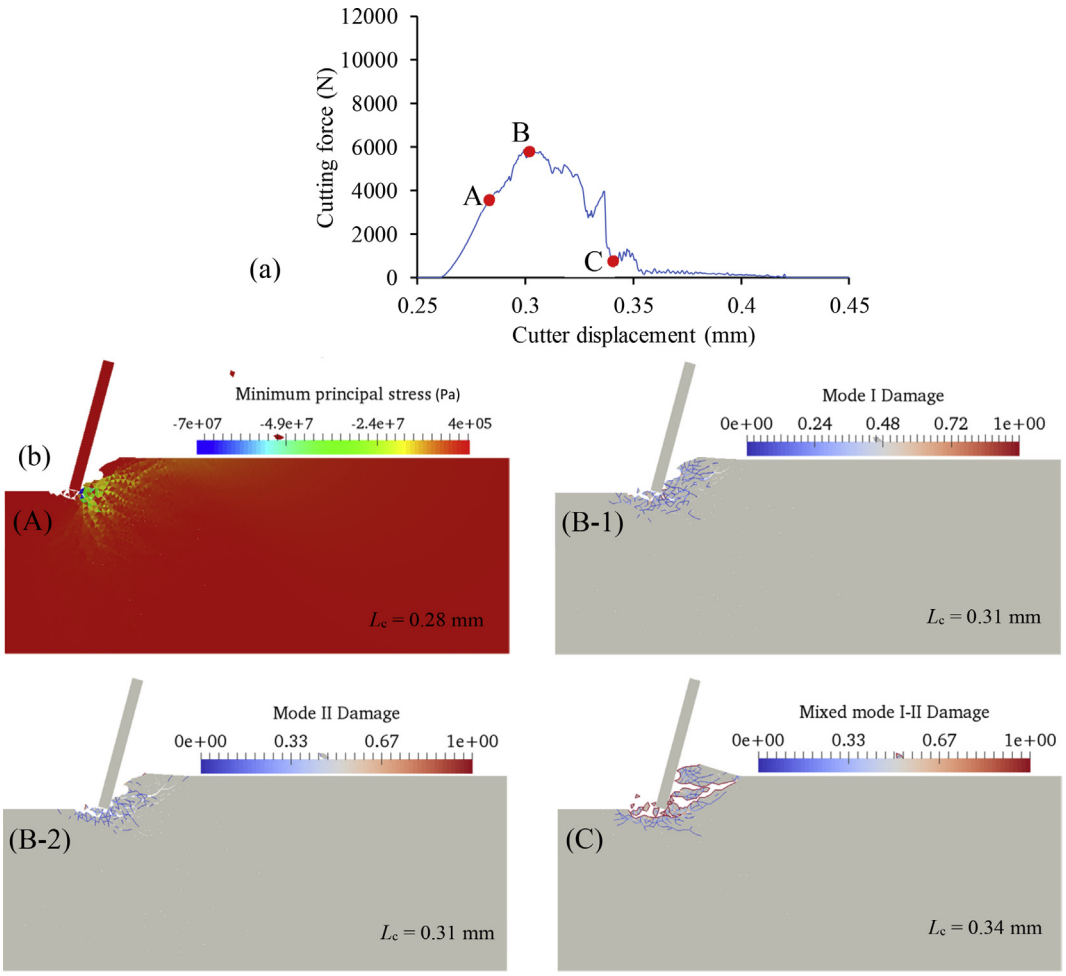


**Fig. 8.** Second chipping process from numerical simulation of the rock scratch test: (a) Force-displacement curve; and (b) Snapshots of the second rock chipping process: (A) Stress field build-up; (B-1) Mode I crack initiation and propagation; (B-2) Mode II crack initiation and propagation; and (C) Chipping due to mixed mode I-II fracturing.

categorised into four stages including: (1) rock deformation and generation of crushed zone near the rock cutting tool; (2) crack initiation and propagation from the boundary of the crushed zone; (3) crack coalescence and chip creation; and (4) chip separation (Fig. 1c).

The rock chipping process in a micro-scale is extremely complex. Based on the acoustic emission observations of rock, many micro-cracks initiate and coalesce prior to the formation of a dominant macro-fracture that can lead to the final failure in both tensile and compression loading conditions (Anders et al., 2014). The region in which micro-crack initiation and coalescence occur is called the fracture process zone (FPZ). In addition to experimental studies, some efforts have been made to develop analytical solutions for rock chipping problems (Evans, 1958; Nishimatsu, 1972), which are mostly developed for quantitative estimation of the cutting force based on the two fundamental assumptions. While Evans (1958) believed that the chipping process is governed by tensile failure, others such as Nishimatsu (1972) considered shearing as the governing mechanism of the rock chipping. It is clear that simplifying the rock chipping process without taking into account rock types and cutting specifications can cause unrealistic estimation of the cutting force. Although the mechanism behind rock chipping remains as an open question in spite of all efforts, it can be concluded that the rock chipping process is due to the dualistic action of shear and tensile fractures; different types of failures may occur in the process (Cox et al., 2005; Tang and Hudson, 2010; Helmons et al., 2016).

### 2.2. Numerical methods for modelling rock failure in mechanical cutting

Precise capturing of onset of rock chipping is a challenging task in experiments. Fortunately, recent advances in computational mechanics have facilitated a much better understanding of the rock fracture process in mechanical cutting. For a realistic simulation of the fracture process, numerical techniques should be able to model crack onset and arbitrary crack growth, correct crack length within a given time interval as well as propagating directions, but not all of the numerical methods can meet these requirements (Mohammadnejad et al., 2018). Till now, the rock failure process in mechanical cutting has been extensively investigated using different numerical techniques although most of them are incapable of modelling the complete rock chipping and fragmentation process. A relatively comprehensive review on the methods and their capabilities can be found in Jaime (2011), Menezes (2017) and Menezes et al. (2014), which shows almost all numerical methods including the finite difference method (Stavropoulou, 2006), the finite element method (FEM) (Liu et al., 2008; Wang et al., 2011), the boundary element method (BEM) (Karekal, 2012) and the discrete element method (DEM) (Lunow

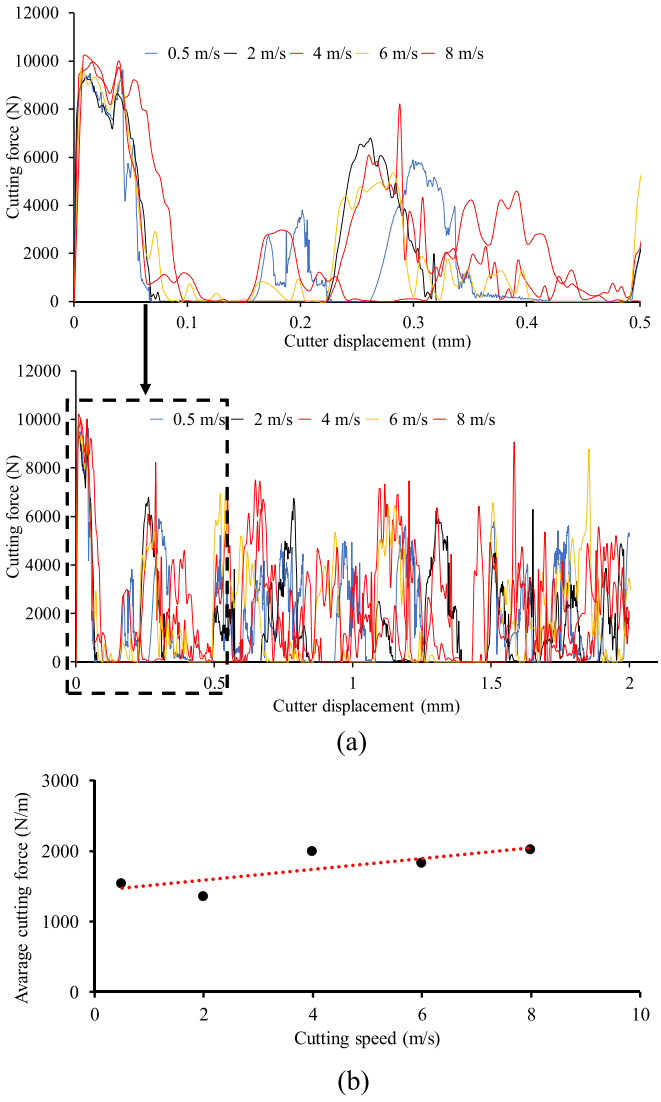


**Fig. 9.** Numerical simulation of the rock scratch tests with various cutting velocities: (a) Cutter force–cutting displacement history; and (b) Variation of average cutting force with the cutting velocity.

and Konietzky, 2009; Huang et al., 2013; Helmons et al., 2016) which are implemented to model the rock chipping process although many of them are unable to model explicit fractures and chip separations. Overall, only two methods have been successfully employed in simulating the full process of chip formation and separation, i.e. the explicit FEM using the element erosion (deletion) algorithms and bonded particle model (BPM). The former method models the fracturing process with a set of deleted (eroded) elements, through which the damage mechanics-based element deletion criteria have been implemented, together with complicated material models, in commercial software such as LS-DYNA and ABAQUS. This method has been employed relatively widely in order to investigate the rock chipping process in mechanical cutting (Yu, 2005; Cho et al., 2010; Menezes et al., 2014; Zhou and Lin, 2014; Jaime et al., 2015; Li and Du, 2016; Shao, 2016; Lu et al., 2017; Menezes, 2017; Xia et al., 2017; Xiao et al., 2017). Being highly mesh dependent and non-convergent in terms of the resultant fracture pattern, this technique can conserve neither mass nor momentum balances in deleted elements. In addition, calibration of the complicated strain or stress failure models can be a very time-consuming process. BPM is a widely used particle-based DEM to model the fracturing process of rocks in mechanical cutting. This method divides the rock domain into circular (two-dimensional (2D)) and spherical (three-dimensional (3D)) rigid elements that are distributed non-uniformly and bonded by cohesive force, obeying Newton's second law. Successful calibrations and applications of BPM in simulation of the rock chipping process have been extensively reported in the literature (e.g. Lei et al., 2004; Thuro and Schormair, 2008; Huang and Detournay, 2013; Huang et al., 2013; Mendoza Rizo, 2013; Li et al., 2015; Zhang et al., 2015; Zhu et al., 2017; Lv et al., 2017; Liu et al., 2018a). Moreover, Mendoza Rizo (2013) proposed a framework for application of BPM to simulating the rock cutting process, and pointed out that the damping coefficient and the cutting speed would be the two key parameters affecting both the mechanism of rock chipping and cutting force significantly. However, the main drawbacks of this technique include particle size dependency in both stages of simulation and calibration, overestimation of tensile strength, reliance on linear failure envelope and difficulties in the modelling of complex geometries (Mohammadnejad et al., 2018). Meanwhile, in the recent two decades, combined numerical techniques have been developed rapidly for rock fracture analysis; these enjoy the advantages of both continuum and discontinuum methods and can deal with the transition from continuum to discontinuum during the rock fracture process. The main types of combined models in rock mechanics are the combination of the BEM/FEM, FEM/DEM, BEM/DEM and the recently developed numerical manifold method (NMM). Not all of the combined methods are suitable for modelling fracture mechanics problems, especially rock chipping and the fragmentation process in mechanical cutting. Aresh (2012) and Mohammadnejad et al. (2017) investigated the capability of FDEM in simulation of rock chipping process. Li et al. (2018) and Liu et al. (2018b) successfully applied NMM to simulating the rock chipping process. Nevertheless, none of them could phenomenologically explain the rock chipping mechanism with failure modes and chip morphology taken into account. To model the mechanism of rock chipping, it is essential that a numerical technique captures the full rock failure process, which is crack initiation, crack propagation, crack branching and crack coalescence from micro-to macro-scales, in which not only mode I fractures but also mode II and mixed mode I-II fractures could take place. Moreover, it should also be capable of modelling the cyclic chipping process which requires a tremendously longer simulation time. This paper proposes the application of FDEM, which can take into account all the aforementioned requirements, in simulating the full rock chipping process. Additionally, the GPGPU parallelisation scheme is incorporated into the applied FDEM code; this makes the whole simulation time significantly shorter, facilitating the simulation of several cycles of chipping.

## 3. Numerical method and calibration of its input parameters

A combined FDEM was initially proposed by Munjiza (2004) and is further developed by several groups (e.g. Munjiza, 2004; Liu et al., 2015; Rougier et al., 2015; Solidity, 2017; Lisjak et al., 2018; Fukuda et al., 2019a, b) around the world. This paper uses Y-HFDEM, an extended version of FDEM, which is firstly developed by the authors (Liu et al., 2015) on the basis of the CPU (central processing unit) based sequential open-source libraries. The code is further parallelised by the authors (Fukuda et al., 2019a, b), using the CUDA (computing unified device architecture) based GPGPU scheme.

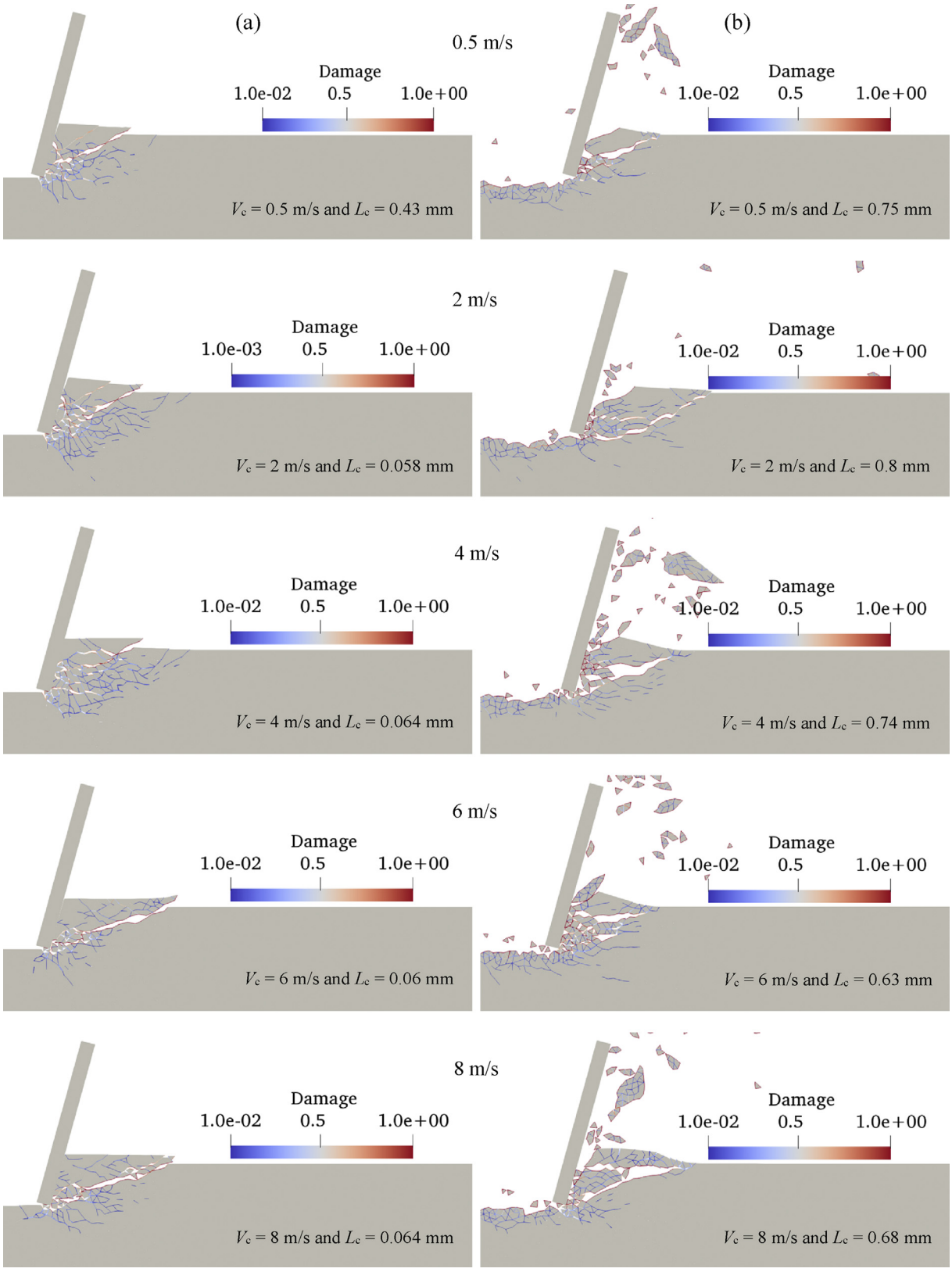


**Fig. 10.** Comparison of rock chippings resultant from the numerical simulations of the rock scratch tests with various cutting velocities: (a) Rock chipping from the first perfect tool-rock engagement; and (b) Rock chipping from the second cyclic imperfect tool-rock engagement.

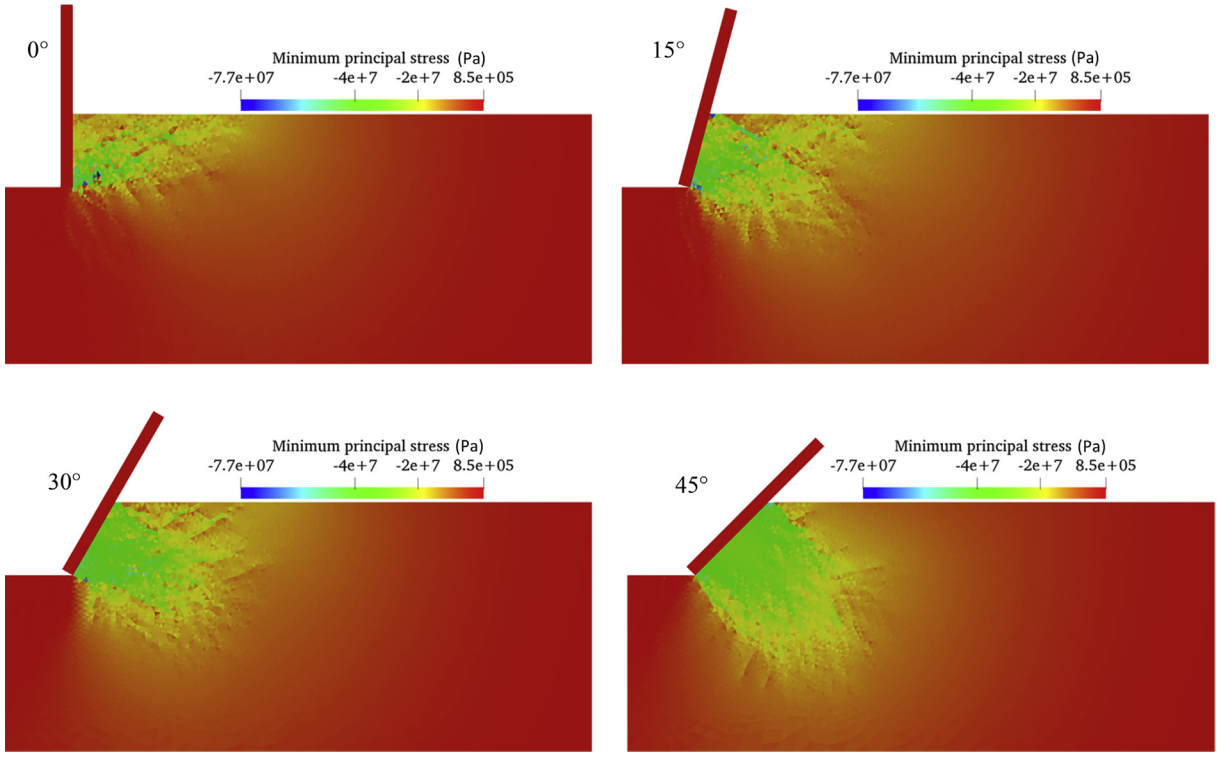


**Fig. 11.** Distribution of the minimum principal stresses from the numerical simulations of the scratch tests with various rake angles ($d$ = 0.6 mm).

### 3.1. GPGPU-parallelised FDEM

The principles of the FDEM are based on continuum mechanics, cohesive zone modelling and contact mechanics, all of which are formulated in the framework of explicit FEM (Munjiza, 2004). The continuum isotropic elastic behaviour of materials is modelled by an assembly of continuum 3-node triangular finite elements (TRI3s) (Fig. 2a), while transition from continuum to discontinuum is modelled through the cohesive zone model (CZM) with the concept of smeared crack (Munjiza et al., 1998). To model the behaviour of the FPZ in front of the crack tips, tensile and shear softening is applied using an assembly of 4-node initially zero-thickness cohesive elements (CE4s) (Fig. 2a) as a function of crack opening and sliding displacements ($o$, $s$), respectively (Fig. 2b). This technique uses the intrinsic cohesive zone model (ICZM) in which the CE4s are imbedded into all the boundary of the TRI3s at the beginning of the analysis. This paper uses one implementation of FDEM, named as Y-HFDEM code, which is sped up by the GPGPU parallelisation scheme (Fukuda et al., 2019a). The normal and shear cohesive tractions ($\sigma^{\mathrm{coh}}$ and $\tau^{\mathrm{coh}}$, respectively), acting on each face of CE4, are computed using Eqs. (1) and (2) assuming tensile and shear softening behaviours, respectively:

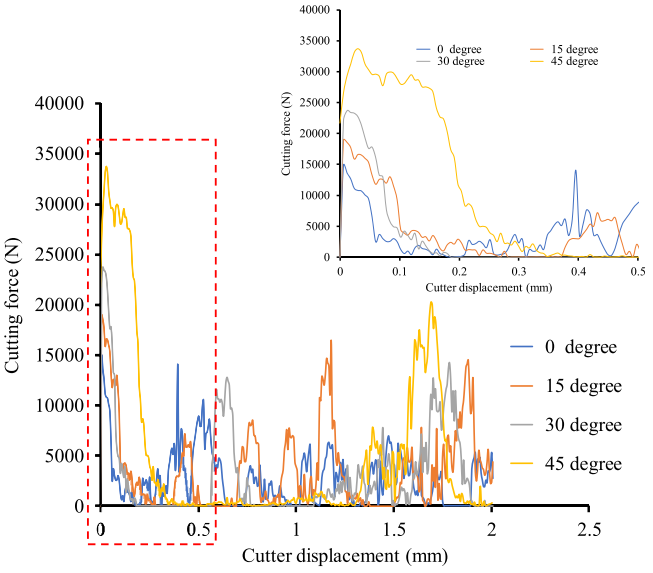


**Fig. 12.** Cutting force-displacement history from the numerical simulations of the scratch tests with various rake angles.

$$\sigma^{\mathrm{coh}} = \begin{cases} \dfrac{2o}{o_{\mathrm{overlap}}} T_{\mathrm{s}} & (o < 0) \\ \left[\dfrac{2o}{o_{\mathrm{p}}} - \left(\dfrac{o}{o_{\mathrm{p}}}\right)^2\right] f(D) T_{\mathrm{s}} & (0 \le o \le o_{\mathrm{p}}) \\ f(D) T_{\mathrm{s}} & (o_{\mathrm{p}} < o) \end{cases} \tag{1}$$

$$\tau^{\mathrm{coh}} = \begin{cases} \left[\dfrac{2|s|}{s_{\mathrm{p}}} - \left(\dfrac{|s|}{s_{\mathrm{p}}}\right)^2\right] \left[ - \sigma^{\mathrm{coh}} \tan\phi + f(D) c\right] & (0 \le |s| \le s_{\mathrm{p}}) \\ -\sigma^{\mathrm{coh}} \tan\phi + f(D) c & (s_{\mathrm{p}} < |s|) \end{cases} \tag{2}$$

where $o_{\mathrm{p}}$ and $s_{\mathrm{p}}$ are the elastic limits of $o$ and $s$, respectively; $o_{\mathrm{overlap}}$ is the representative overlapping when $o$ is negative; $T_{\mathrm{s}}$ is the tensile strength of CE4; $c$ is the cohesion of CE4; and $\phi$ is the internal friction angle of CE4. Positive values of $o$ and $\sigma^{\mathrm{coh}}$ indicate crack opening and tensile cohesive traction, respectively. Eq. (2)

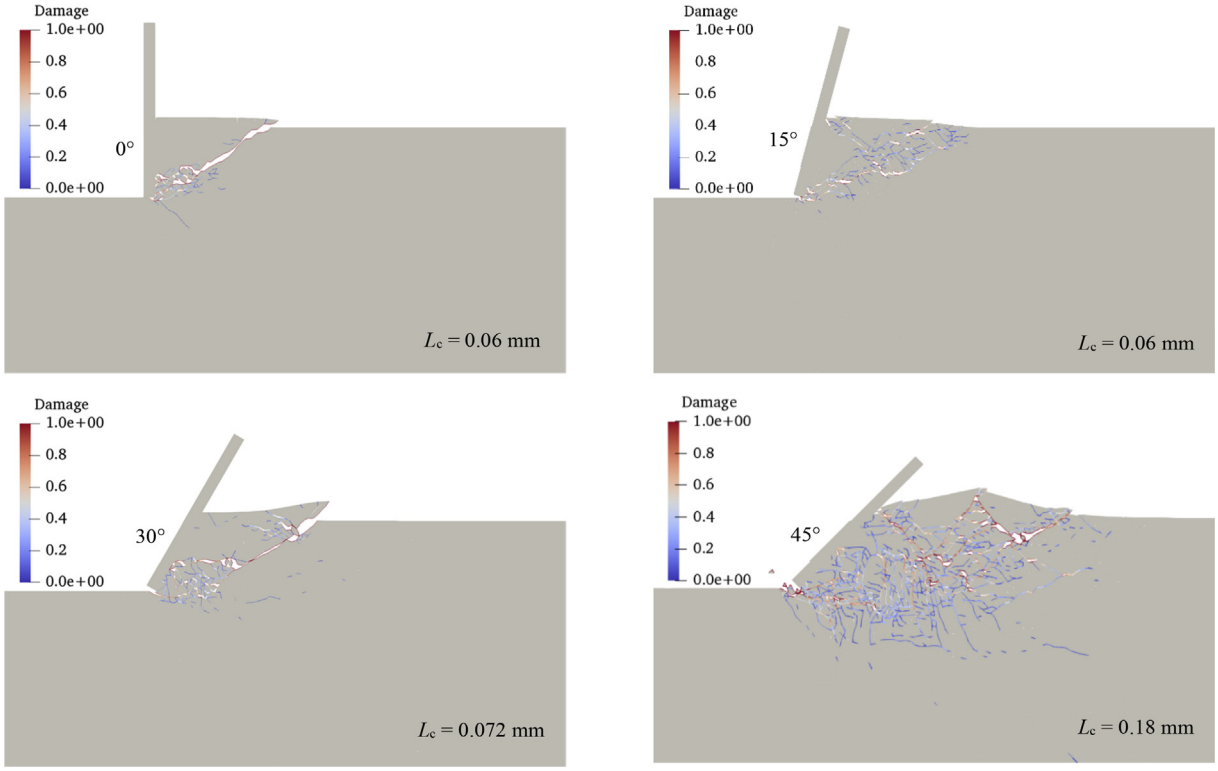


**Fig. 13.** Rock chipping process from the numerical simulations of the scratch tests with various rake angles.

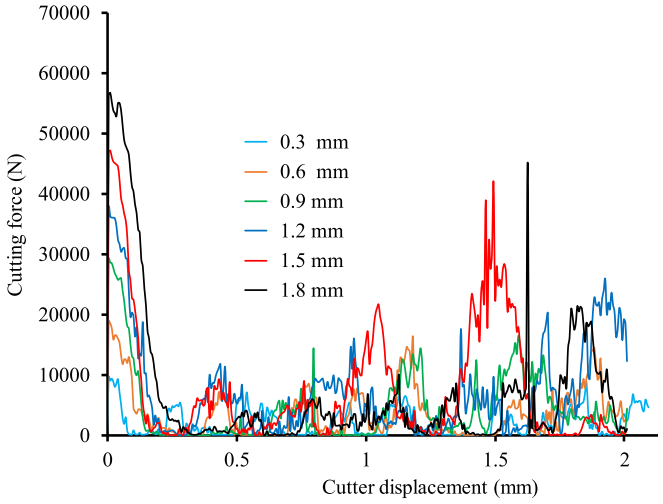


**Fig. 14.** Cutting force-displacement history from the numerical simulations of the scratch tests with various cutting depths.

corresponds to the Mohr-Coulomb (MC) shear strength model with tension cut-off. The "artificial" stiffnesses of each CE4 are $P_f$, $P_{tan}$ and $P_{overlap}$ for its opening in normal direction, sliding in tangential direction and overlapping in normal direction, respectively. The function, $f(D)$, in Eqs. (1) and (2) is the characteristic function for tensile and shear softening curves (Fig. 2b), depending on a damage value $D$ of the CE4. The following definition of $D$ is used to consider the modes I and II fracturing as well as a mixed mode I-II fracturing (Munjiza et al., 1998; Mahabadi et al., 2012):

$$D = \min\left(1,\ \sqrt{\left(\frac{o-o_p}{o_t}\right)^2 + \left(\frac{|s|-s_p}{s_t}\right)^2}\right) \quad (\text{if } o \geq o_p \text{ or } |s| > s_p,\ \text{otherwise } 0) \tag{3}$$

where $o_t$ and $s_t$ are the critical values of $o$ and $s$, respectively, in which a CE4 breaks and turns to a macro/explicit fracture. The $o_t$ and $s_t$ in Eq. (3) satisfy the modes I and II fracture energies $G_{fI}$ and $G_{fII}$ specified in Eqs. (4) and (5), respectively:

$$G_{fI} = \int_{o_p}^{o_t} \sigma^{coh}(o)\mathrm{d}o \tag{4}$$

$$G_{fII} + W_{res} = \int_{s_p}^{s_t} \tau^{coh}(|s|)\mathrm{d}|s| \tag{5}$$

where $W_{res}$ is the amount of work per area of CE4 done by the residual stress term in the MC shear strength model. In this paper, mode I damage is the value of $D$ in Eq. (3) defined under the condition that $o \geq o_p$ and $|s| < s_p$ while mode II damage is the value of $D$ in Eq. (3) satisfying $o < o_p$ and $|s| \geq s_p$. The value of $D$ in Eq. (3) under all other conditions is mixed mode damage.

The parallel programming scheme is implemented on the basis of GPGPU using CUDA C/C++, in which the computation on the GPGPU device is controlled through CUDA C/C++ and a greater degree of parallelism occurs within the GPGPU device itself. Functions, also known as "kernels", are launched on the GPGPU device and are executed by many "threads" in parallel. A "thread" is

just an execution of a "kernel" with a given "thread index" within a particular "block". A "block" is a group of threads, and a unique "block index" is given to each "block". The "block index" and "thread index" enable each thread to use its unique "index" to access elements globally in the GPGPU data array, such that the collection of all threads processes the entire data set in a massively parallel manner. In each "thread" level, the corresponding code that the "threads" execution is very similar to the CPU-based sequential code, which is one of the advantages of the application of CUDA C/C++. In the subsequent GPGPU-parallelised FDEM modelling, the rock specimen is discretised using triangular mesh. The 4-node cohesive elements are inserted between adjacent triangular elements which damage and fracture according to Eq. (3). The computations for each triangular element, cohesive element, contact couple or nodal motion are assigned to each GPGPU kernel and processed in a massively parallel manner. The contact detection algorithm divides the analysis domain into multiple sub-cells with the size of each sub-cell being at least greater than the largest triangular element. It implements a radix sorting algorithm to sort the triangular elements in the sub-cells for contact detection of the triangular elements in a particular sub-cell and its adjacent sub-cells, which is also processed in a massively parallel manner. The detailed GPGPU parallel implementation of the Y-HFDEM2D/3D IDE code can be found in Fukuda et al. (2019a, b), which is omitted here. The detailed computing performance analysis of the GPGPU-parallelised Y-HFDEM IDE code by Fukuda et al. (2019a, b) indicates that it can achieve the maximum speedups of 128.6 and 286 times in the case of the 2D and 3D modellings, respectively.

The FDEM implements the fracture mechanics (energy failure criterion) and damage mechanics principles to model the rock chipping and fragmentation process. By not using bonded circular or spherical particles like BPM or the erosion algorithms like explicit FEM, FDEM does not suffer from poorly simulated crack paths (Song et al., 2008) or from unrealistic simulation of the brittle failure of rock (Nakashima et al., 2016). However, similar to all mesh-based numerical methods, the FDEM suffers from mesh size and mesh bias dependency. This drawback can be alleviated by using fine mesh sizes (Munjiza and John, 2002), which increases simulation time significantly. Accordingly, the parallelisation scheme, as briefly described above and detailed in Fukuda et al. (2019a, b), is necessary to increase computational speed and to make the numerical simulation affordable. Section 4 aims to show the significant potential of the proposed GPGPU-parallelised FDEM for making numerical simulations of the rock cutting process.

### 3.2. Determination of model parameters

An appropriate determination of the model parameters is essential for accurate simulation of the rock cutting process using FDEM. In this study, the model parameters are calibrated against two standard laboratory rock mechanics tests, i.e. BTS and UCS tests on limestone specimens. The physical and mechanical properties of the limestone and the input parameters used in the numerical simulations of BTS and UCS tests are listed in Table 1. This study follows the calibration process suggested by Tatone and Grasselli (2015) and uses density ($\rho$), Young's modulus ($E$) and Poisson's ratio ($\nu$) determined from the experiments. The penalty numbers are calibrated to satisfy the elastic response of the rock and then the strength parameters are determined by capturing the appropriate fracture pattern and the complete stress–strain curve. This study departs from Tatone and Grasselli (2015) methodology when the strength parameters are not tuned to yield to pure tensile and shear damages in the BTS and UCS tests. This study uses unstructured mesh in the FDEM simulations and authors believe that pure mode I and mode II cracks are highly unlikely due to the topological restriction when unstructured mesh is used. When structured mesh is used, since CE4s have planes exactly aligned with favoured loading direction, pure opening and shearing can take place (see Fig. 3a and b); whilst in the case of unstructured mesh, none of the normals to the planes can align with that of the stress regime, as depicted in Fig. 3c. Thus, mixed mode I-II fracturing is the most probable failure mechanism with unstructured meshes. Based on a comprehensive study conducted by Tijssens et al. (2000), the fractures tend to propagate along the dominant directions of the local mesh alignment. Therefore, any intentional change in the strength parameters to capture the unreasonable pure mode I or mode II fracture can result in unrealistic results, contradicting the principles of CZM. Pure mode I and mode II micro-cracks can be initiated in the models with unstructured mesh only when the conditions depicted in Fig. 3a and b, respectively, are satisfied. Finally, the critical damping ($\eta_{\text{crit}}$) in modelling is estimated through $\eta_{\text{crit}} = 2h\sqrt{\rho E}$ (Munjiza, 2004), where $h$ is the mesh size.

In the UCS numerical model, the height and diameter of the rock specimen are 129.5 mm and 51.7 mm, respectively, and in the BTS numerical model, the diameter of the rock disc is 51.7 mm. The average edge length, $h_{\text{ave}}$, of TRI3s in both models for the BTS and UCS tests is 0.7 mm. The rock specimens are placed between two moving rigid platens with a constant velocity of 0.05 m/s to satisfy quasi-static loading conditions. The geometries of the BTS and UCS tests are shown in Fig. 4a and Fig. 5b, respectively. Sensitivity analysis of element size and platen velocity conducted by the authors, as well as that reported by Tatone and Grasselli (2015) and Liu and Deng (2019), has shown that the selected element size of 0.7 mm does not affect the result, and neither does the assigned platen velocity. The friction coefficient, $\mu_{\text{fric}}$, between the loading platens and the rock specimens and that between broken cohesive elements are assumed to be 0.1 and 0.5, respectively, based on the study of Fukuda et al. (2019a).

Fig. 4b depicts the modelled indirect tensile stress versus the vertical displacement curve while the distribution of the horizontal stress, $\sigma_{xx}$, and the damage variable is illustrated in Fig. 4c. In Fig. 4b, compressive stress is shown as negative (cold colour) while tensile stress is regarded as positive (warm colour). In damage profiles, colour represents the relative size of the damage variable. These sign conventions are used throughout the paper. Fig. 4c A corresponds to the snapshot of the failure process taken at point $A$ in Fig. 4b before the macroscopic splitting/tensile failure is initiated. Since some mode II damage occurs at this point and correspondingly some shear micro-cracks are initiated in the contact area between the rock disc and the loading platens. However, it should be noted that no macro-cracks appear at this stage since the damage variable is much smaller than 1. When the indirect tensile stress along the central line of the disc reaches the peak value, which corresponds to point $B$ in Fig. 4b, tensile (mode I) micro fractures are initiated approximately along the central line of the model, as shown in Fig. 4c B-2, where model I damage variable is depicted. It is noted again that no macro-crack appears at this stage since the damage variable is still smaller than 1. When the loading platens narrow down further, macroscopic splitting cracks (Fig. 4c C-1) are formed approximately along the central line of the Brazilian disc due to the accumulation, propagation and coalescence of the initiated micro-cracks in previous stages. The mixed mode fractures (Fig. 4c C-2) are the dominant mechanism during the propagation and coalescence of the initiated model I micro-cracks that form the macroscopic splitting cracks. Thus, although the micro-fractures are initiated mostly in mode I, when the indirect tensile stress reaches the tensile strength, the final macroscopic fractures are not necessarily formed in mode I and can be of mixed

mode I-II, especially when unstructured mesh discretization is used.

Axial stress–strain curve obtained from the modelling of the UCS test is shown in Fig. 5b. The minimum principal stress evolution and corresponding rock fracture process are also shown in Fig. 5c. As shown, the stress and resultant micro-cracks are uniformly distributed within the specimen during the initial loading stage and the corresponding stress–strain curve is almost linear until point *A* in Fig. 5b. It can be seen from Fig. 5b A-2 that the mode II damage is the dominant micro-cracking mechanism. As loading platens narrow down further, micro-crack coalescence and localisation occur. This results in nonlinear stress–strain behaviour from the point *A* to point *B* (Fig. 5b). The corresponding distributions of the minimum principal stress and the micro-cracks are illustrated in Fig. 5c B-1 and B-2, respectively. As shown, shear failure is the dominant damage mechanism. After this point, the coalescence and localisation of the micro-cracks lead to initiation of macro-cracks and correspondingly the rock specimen loses its bearing capacity, as shown in Fig. 5b C. At the same time, the initiated macro-cracks further propagate resulting in a diagonal fracture pattern, as shown in Fig. 5c C. During the propagation of the macro-cracks, the mixed mode damage is the failure mechanism although the shearing failure plane is still dominated by the model II damages. The final fracture pattern is compared with that obtained results from the aforementioned experimental UCS test of limestone, as shown in Fig. 5d.

## 4. Numerical simulation of rock cutting and discussion

The scratch test can be simulated under the plane strain mode, since the rock thickness is much larger than the cutting depth (Jaime, 2011) while the out-of-place stress is neglected. Similar to prior literature (Huang and Detournay, 2008; Menezes, 2017), the numerical model of the rock scratch test is simplified as a rock slab and a rigid cutter moving across the rock slab, as shown in Fig. 6. The smallest model with the shallowest cutting depth has 44,719 triangular elements, 112,117 cohesive elements, and 134,157 nodes while the largest model with the deepest cutting depth has 154,224 triangular elements, 385,963 cohesive elements and 462,672 nodes, which make it impossible for the traditional sequential FDEMs to complete these rock cutting simulations, especially considering that many cycles of rock–cutter interaction are modelled in them. The input parameters in Table 1 calibrated against those of the limestone are used for the rock slab. The cutter is modelled as a rigid material with different rake angles (0°, 15°, 30° and 45°) and cutting velocities (0.5 m/s, 2 m/s, 4 m/s, 6 m/s and 8 m/s). Six cutting depths (0.3 mm, 0.6 mm, 0.9 mm, 1.2 mm, 1.5 mm and 1.8 mm) are investigated in the subsequent numerical simulations. The elements' size of 0.05 mm is used for both the cutter and the rock slab. The bottom, right and left boundaries of the rock slab are fixed, while the cutter is forced to move only along horizontal direction at a constant set speed.

### 4.1. Failure mechanism

The rock chipping process obtained numerically with a rake angle of 15°, cutting depth of 0.3 mm and cutting velocity ($V_c$) of 0.5 m/s is shown in Fig. 7. The corresponding cutting force-cutter displacement ($L_c$) history is depicted in Fig. 7a. Frequent drops in the cutting force history are also observed in rock cutting experiments characterizing the sequences of the cutter engagement and the cutter detachment (Richard et al., 1998). As shown in Fig. 7a, the cutting force increases until the explicit fracture develops in the model and then falls to zero with the detachment of rock fragments from the cutter, resulting in chip formation. The action of cutter on the surface of the rock slab concentrates stress on the contact region between the rock slab and the cutter in Fig. 7b A. Here compression is negative and tension is positive. As can be seen, as the cutter compresses the rock, it induces compressive stress in the vicinity of the contact face between the cutter and the rock, which corresponds to peak point in the cutting force-displacement curve in Fig. 7a. As the cutter displacement increases, the cutting force reaches its first peak at point *B* in Fig. 7i and mode II micro-cracks are initiated within the compressed zone ahead of the cutter. These cracks form the crushed zone, which has significant influences on the formation of the subsequent fracturing system. As the displacement further increases, the coalescence of multiple micro-cracks leads to creation of a chipping crack that extends unstably to the free surface (Fig. 7b C). At this stage, the final chip forms due to the propagation of an unstable mixed mode I-II fracture, as shown in Fig. 7b C, followed by chip separation, which is the formation of rock fragments. Under perfect tool-rock contact, shearing failure seems to be the main failure mechanism, since the stress state is of compression and mode II cracks are dominant, although the final chip is formed due to the mixed mode failure mechanism.

As cutting proceeds, the cutter-rock contact interface becomes smaller due to uneven contact area. As shown in Fig. 8b A, unlike the previous cycle, both relatively large compressive stresses (cold colour) and tensile stresses (warm colour) are induced in the model. This leads to a limited number of mode II cracks being initiated near the cutter (Fig. 8b B). As the cutter moves further, unstable mode I (tensile) micro-cracks are developed in the model (Fig. 8b C). This, with coalesce and extension of mode I-II macro-fractures, forms the second round of chipping. The obtained results from the hybrid FDEM simulation acknowledge the findings reported by Jaime (2011) and Tan et al. (1998) who also found that the formation of the chip is due to the action of multiple fracture mechanisms. Additionally, it is evident that tool-rock interaction is a key factor affecting the morphology of the chips and the corresponding cutting force-displacement curve. It is noted that the maximum cutting force in the subsequent tool-rock engagements is ~6 kN compared with that of 10 kN in the first chipping process. The size of the fragments formed is not noticeably different though. This is likely that the cutting is more efficient in the follow-on chipping process in which tensile cracks contribute significantly to the breakage. Moreover, the hybrid FDEM modelling demonstrates that the failure mechanism of the chipping process and the cutting force in mechanical cutting are particularly a function of tool-rock interaction and the assumption of a single failure mechanism for the chipping process may lead to misinterpretations and incorrect estimations.

### 4.2. Effect of cutting velocity

The effect of cutting velocity on the cutting force and chip formation is modelled by considering a range of cutter velocities of 0.5 m/s, 2 m/s, 4 m/s, 6 m/s and 8 m/s. Fig. 9 records the cutting force versus the cutting displacement curve for the case of cutting depth of 0.3 mm, at various cutting velocities. In Fig. 9b, the cutting force does not affect the cutting force. On the other hand, with a constant time period, the frequency of engagements between cutter and rock increases with the increasing cutting velocity. The rock fragments' size is, therefore, correlated with the cutting velocity. Fig. 10 compares the sizes of the fragments generated by the cutters at different velocities. The number of micro-cracks initiated in the rock slab increases with increase of cutting velocity. This can be attributed to extra energy of higher cutting velocity that is consumed to generate more new fracture surfaces (Zhang, 2016). In terms of the failure mode, in all cases, the macroscopic cracks leading to chipping are due to the mixed mode I-II fractures. The

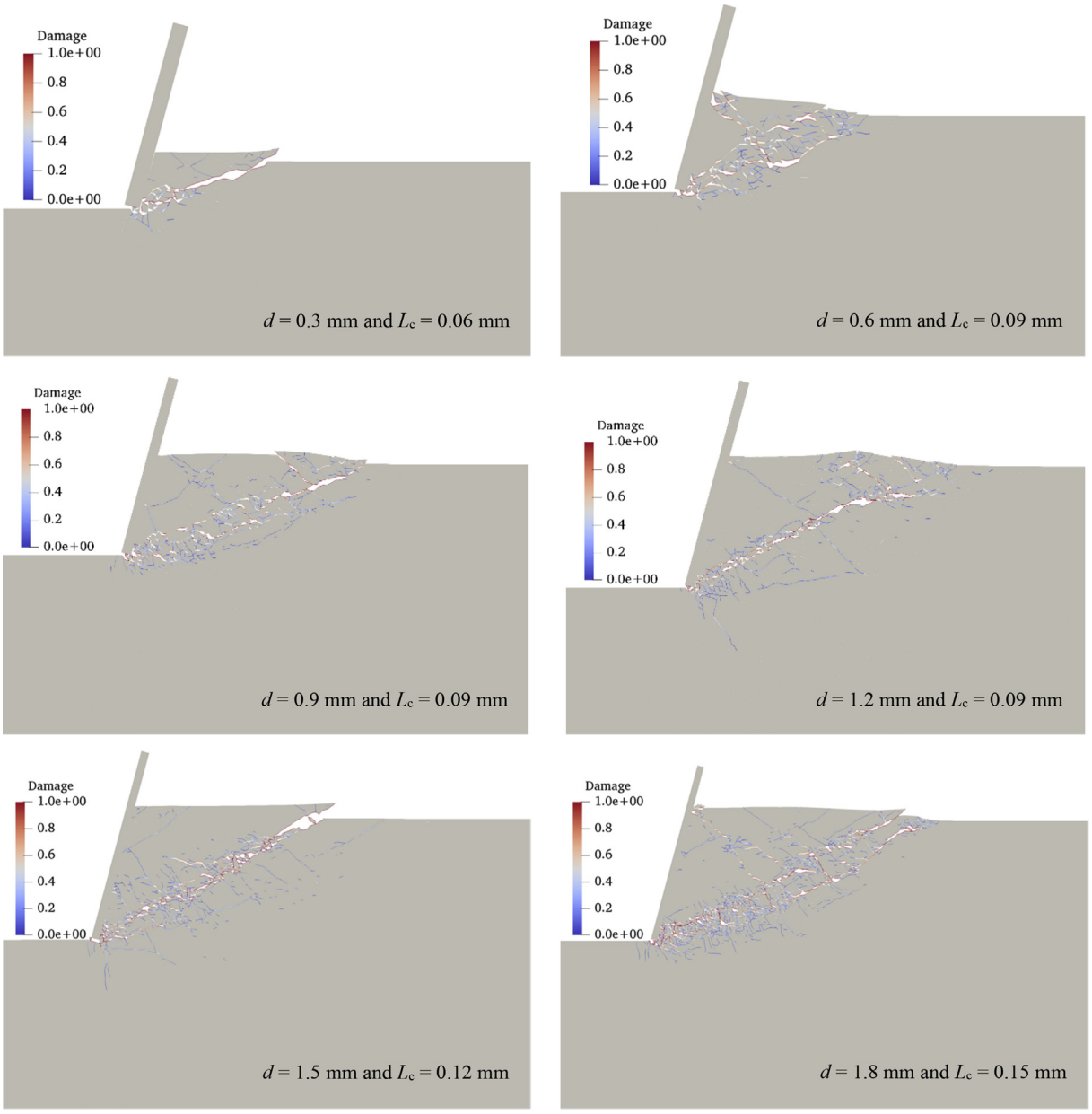


**Fig. 15.** Rock chippings from the numerical simulations of the scratch tests with various cutting depths.

results obtained from these simulations are compatible with those in the literature (Jaime, 2011; Menezes, 2017; Li et al., 2018).

As observed in Fig. 10, ductile failure cannot be captured in current FDEM simulations of shallow cutting, although the dominance of shear failure increases with increase in cutting velocity. Mendoza Rizo (2008) also investigated the effect of the cutting velocity in simulation of the rock scratch test using BPM and concluded that low cutting velocity cannot secure a realistic simulation of ductile failure in shallow depth of cut. He suggested a cutting velocity of 2 m/s, with a damping coefficient of 0.7, for a realistic simulation of the cutting process. Similar observations have been made by Jaime (2011) with FEM simulations of the rock scratch tests, indicating that the cutting forces remained almost unchanged when the cutting velocity increased to more than 2 m/s. Despite these efforts, it remains an open question: to what extent can the cutting velocity be increased? Additionally, how can the damping coefficient be extended and to what point can it be increased so that the negative effect on stress distribution is negligible? Hence, the cutting velocity of 2 m/s is employed in all rock-cutting simulations herein. It should be noted that the input parameters in all rock cutting simulations are selected based on the explained calibration process of UCS and BTS tests, and unlike Mendoza Rizo (2008), no local damping scheme has been used.

### 4.3. Effect of rake angle

The effect of cutter rake angle on rock chipping process is investigated using the models with a constant cutting depth of 0.6 mm at various cutter rake angles (0°, 15°, 30° and 45°). The distribution of the induced stress immediately in front of the cutter-rock contact, as shown in Fig. 11, demonstrates the effect of the rake angle. In the model with a rake angle of 0°, the compressive and tensile stress concentration is close to the free surface, in favour of chip formation. By increasing the rake angle,

the stress tends to concentrate dipper into the rock and the stress state changes to mainly compression mode. Similar trends can be observed in cutting force as shown in Fig. 12. A positive correlation between the rake angle and the mean cutting force is reported by both Menezes (2017) and Lei et al. (2004), where the explicit FEM and BPM models were employed, respectively.

The chipping patterns of cutters at different rake angles are shown in Fig. 13. As the rake angle increases, more micro-cracks are initiated and propagated deep into the rock slab. The micro-cracks are mostly of mode I failures away from the cutter and dipper in the rock, whilst those in the vicinity of the cutting tool are of mode II. The macro-cracks leading to chips are, however, formed due to the mixed mode I-II failures in all cases. Moreover, it is evident that the size of the rock fragments increases with increase of rake angle, although it should be noted that these results are under the provision of ideal contact between rock and cutter and it may differ with different configurations of tool-rock interaction.

### 4.4. Effect of cutting depth

As reviewed in Section 2.1, the cutting depth has an important influence on the rock fragmentation process in mechanical cutting. The effect of the cutting depth on the rock failure mechanism and the associated cutting force is investigated numerically here with a range of cutting depths ranging from 0.3 mm to 1.8 mm, with an interval of 0.3 mm. In these models, cutting velocity and rake angle are kept constant at 6 m/s and 15°, respectively.

Fig. 14 compares the cutting force profiles with respect to cutting displacement at different cutting depths. As expected, a positive correlation is observed between the associated cutting force and the cutting depth. Unfortunately, the simulations have been unsuccessful in demonstrating transition between ductile to brittle cutting models observed in experiments as cutting depth increases. This could be due to the cutting losing engagement with the rock as the fragments escape the cutter front too quickly. The frequent drops in cutting force histories are a result of this phenomenon. This shortcoming is a common with numerical models. Jaime (2011) reported similar results to the hybrid FDEM with explicit FEM code (LS-DYNA), who employed a filtering procedure to compare the explicit FEM modelled force signals with experimental data.

Fig. 15 illustrates the failure patterns obtained from the modelling with various cutting depths. It can be seen that the chip size increases with increase of the cutting depth. Moreover, it is noticed that, in the model with a shallow cutting depth, mode II cracks are the main cause of chipping. This is in agreement with the results reported by Zhou and Lin (2014). It is also evident that the number and extension length of cracks increase as the cutting depth increases. This is especially the case for the sub-surface cracks propagating deep into the rock in a certain angle with respect to the cutter rake angle. Mode II cracks are mostly initiated and propagated from the vicinity of the cutter and chipping region. It is necessary to point out again that the numerical simulation in this study could not capture the ductile (or grinding) failure mechanism of shallow depth of cut, as reported in rock cutting experiments with a shallow cutting depth. Therefore, in all cases, chipping due to extension of mixed mode I-II cracks is the ultimate cutting mechanism. Mendoza Rizo (2013) suggested increasing the local damping coefficient to 0.7, in order to capture the grinding behaviour in a rock cutting simulation using BPM. A similar strategy may be implemented in future studies with the hybrid FDEM used in the present study, as a remedy to allow capturing ductile failure cutting at shallow depth. However, it suggests that care must be taken since high value of damping coefficient may result in unrealistic stress distribution and then unrealistic rock fracturing. Although Zhou and Lin (2014) claimed that they could successfully simulate the ductile–brittle transition process using LS-DYNA, based on their given results, it seems that their failure mechanism obtained was still chipping or brittle failure, which was similar to those in this study. Moreover, they only conducted numerical simulation for a case where there is perfect contact between cutter and rock.

## 5. Conclusions

This study investigates application of a hybrid FDEM, which enjoys the advantages of both FEM and BPM, to modelling the rock chipping and fragmentation process in the rock scratch test of mechanical rock cutting. A self-developed FDEM computing technique, parallelised using GPGPU, is used in the study of chipping and fragmentation process. The input parameters of the numerical model were then calibrated using standard BTS and UCS tests of the limestone. Simulation of cutting experiments has been conducted on the basis of simple rock scratch tests with various cutting velocities, cutter rake angles and cutting depths. A few chipping cycles that include continuous engagement and detachment between the cutter and the rock are modelled for each of the cases. As a result, the failure mechanism, resultant cutting force, and chipping morphology have been evaluated under the effects of the various factors. In this study, the following conclusions can be drawn:

(1) The hybrid FDEM is capable of modelling all four of the stages of the rock chipping and fragmentation process in mechanical rock cutting: (i) stress field build-up; (ii) crack initiation and propagation; (iii) crack coalescence and chipping process; and (iv) chip separation and formation. Unlike explicit FEM and BPM, the hybrid FDEM could capture explicitly, not only different fracture mechanisms contributing to the rock chipping, but also chip formation and separation processes in mechanical cutting. Whilst the GPGPU-parallelised hybrid FDEM provided a powerful tool to study the rock cutting process, further validation is needed against specific experimental tests.

(2) According to the hybrid modelling, the chipping is mostly owing to the mixed mode I-II fracture in all cases, although mode II cracks and mode I cracks are dominant failures in rock cutting with shallow and deep cutting depths, respectively.

(3) The simulations of rock cutting demonstrate that the chip morphology is a function of the cutter velocity, cutting depth and cutter rake angle. While the increases in cutting depth and cutter rake angle result in larger chips, the cutting velocity negatively affects that. As the rake angle increases, more subsurface cracks appear in the rock and accordingly, the cutting force increases. Moreover, with increasing cutting depth, more micro-cracks, mostly of mode I, are initiated, whilst the final chip is the result of a combination of different mechanisms.

(4) Similar to explicit FEM, the hybrid FDEM is unable to capture ductile failure observed in rock cutting experiments at shallow cutting depth. In future studies, the potential of using damping coefficient in hybrid FDEM will be explored to model ductile cutting mode, and it is likely that the increase of the damping coefficient might have other adverse effects.

## Declaration of Competing Interest

We wish to confirm that there are no known conflicts of interest associated with this publication and there has been no significant

financial support for this work that could have influenced its outcome.

## Acknowledgments

The corresponding authors would like to acknowledge the support of CSIRO and the Australia-Japan Foundation (Grant No. 17/20470). The third author of this work is supported by the Japan Society for the Promotion of Science KAKENHI (Grant No. JP18K14165) for Grant-in-Aid for Young Scientists, which is greatly appreciated. Moreover, all authors would like to thank the anonymous reviewers for their helpful and constructive comments that significantly contributed to improving the final version of the paper.

## References

Anders MH, Laubach SE, Scholz CH. Microfractures: a review. Journal of Structural Geology 2014;69:377–94.
Aresh B. Fundamental study into the mechanics of material removal in rock cutting. PhD Thesis. Northumbria University; 2012.
Bazant ZP, Planas J. Fracture and size effect in concrete and other quasibrittle materials. CRC Press; 1997.
Che D, Zhu WL, Ehmann KF. Chipping and crushing mechanisms in orthogonal rock cutting. International Journal of Mechanical Sciences 2016;119:224–36.
Cho JW, Jeon S, Yu SH, Chang SH. Optimum spacing of TBM disc cutters: a numerical simulation using the three-dimensional dynamic fracturing method. Tunnelling and Underground Space Technology 2010;25:230–44.
Cox BN, Gao H, Gross D, Rittel D. Modern topics and challenges in dynamic fracture. Journal of the Mechanics and Physics of Solids 2005;53:565–96.
Detournay E, Atkinson C. Influence of pore pressure on the drilling response in low-permeability shear dilatant rocks. International Journal of Rock Mechanics and Mining Sciences 2000;37(7):1091–101.
Detournay E, Defourny P. A phenomenological model for the drilling action of drag bits. International Journal of Rock Mechanics and Mining Sciences & Geomechanics Abstracts 1992;29(1):13–23.
Evans I. Theoretical aspects of coal ploughing. In: Mechanical properties of non-metallic brittle materials. Butterworths; 1958. p. 451–68.
Fukuda D, Mohammadnejad M, Liu H, Dehkhoda S, Chan A, Cho SH, Min GJ, Han H, Kodama J, Fujii Y. Development of a GPGPU-parallelized hybrid finite-discrete element method for modeling rock fracture. International Journal for Numerical and Analytical Methods in Geomechanics 2019a;43:1797–824.
Fukuda D, Mohammadnejad M, Liu HY, Zhang Q, Zhao J, Dehkhoda S, Chan A, Kodama J, Fujii Y. Development of a 3D hybrid finite-discrete element simulator based on GPGPU-parallelized computation for modelling rock fracturing under quasi-static and dynamic loading conditions. Rock Mechanics and Rock Engineering 2019. https://doi.org/10.1007/s00603-019-01960-z.
He XQ, Xu CS. Discrete element modelling of rock cutting: from ductile to brittle transition. International Journal for Numerical and Analytical Methods in Geomechanics 2015;39:1331–51.
He X, Xu C. Specific energy as an index to identify the critical failure mode transition depth in rock cutting. Rock Mechanics and Rock Engineering 2016;49:1461–78.
He X, Xu C, Peng K, Huang G. Simultaneous identification of rock strength and fracture properties via scratch test. Rock Mechanics and Rock Engineering 2017;50:2227–34.
Helmons R, Miedema SA, van Rhee C. Modelling the effect of water depth on rock cutting processes with the use of discrete element method. Terra et Aqua 2016;142:17–24.
Hood M, Alehossein H. A development in rock cutting technology. International Journal of Rock Mechanics and Mining Sciences 2000;37:297–305.
Huang H, Detournay E. Intrinsic length scales in tool-rock interaction. International Journal of Geomechanics 2008;8(1):39–44.
Huang H, Detournay E. Discrete element modeling of tool-rock interaction. II: rock indentation. International Journal for Numerical and Analytical Methods in Geomechanics 2013;37:1930–47.
Huang H, Lecampion B, Detournay E. Discrete element modeling of tool-rock interaction. I: rock cutting. International Journal for Numerical and Analytical Methods in Geomechanics 2013;37:1913–29.
Jaime MC. Numerical modeling of rock cutting and its associated fragmentation process using the finite element method. PhD Thesis. University of Pittsburgh; 2011.
Jaime MC, Zhou Y, Lin JS, Gamwo IK. Finite element modeling of rock cutting and its fragmentation process. International Journal of Rock Mechanics and Mining Sciences 2015;80:137–46.
Karekal S. Modeling rock chipping process in linear drag cutting mode. In: ISRM international Symposium – EUROCK 2012, stockholm, Sweden. International Society for Rock Mechanics and Rock Engineering (IRSM); 2012.
Lei S, Kaitekay P, Shen X. Simulation of rock cutting using distinct element method-PFC2D. In: Numerical modelling in micromechanics via particle methods. London, UK: Taylor and Francis Group; 2004.
Li H, Du E. Simulation of rock fragmentation induced by a tunnel boring machine disk cutter. Advances in Mechanical Engineering 2016;8(6). https://doi.org/10.1177/1687814016651557.
Li B, Chen W, Liu X, Li L. Discrete element simulation of attenuation law of blasting stress wave. In: Proceedings of the international conference on chemical. Material and Food Engineering; 2015.
Li X, Zhang Q, Li J, Zhao J. A numerical study of rock scratch tests using the particle-based numerical manifold method. Tunnelling and Underground Space Technology 2018;78:106–14.
Lisjak A, Mahabadi OK, He L, Tatone BSA, Kaifosh P, Haque SA, Grasselli G. Acceleration of a 2D/3D finite-discrete element code for geomechanical simulations using General Purpose GPU computing. Computers and Geotechnics 2018;100:84–96.
Liu Q, Deng P. A numerical investigation of element size and loading/unloading rate for intact rock in laboratory-scale and field-scale based on the combined finite-discrete element method. Engineering Fracture Mechanics 2019;211:442–62.
Liu H, Kou S, Lindqvist PA. Numerical studies on bit-rock fragmentation mechanisms. International Journal of Geomechanics 2008;8:45–67.
Liu HY, Kang YM, Lin P. Hybrid finite-discrete element modeling of geomaterials fracture and fragment muck-piling. International Journal of Geotechnical Engineering 2015;9:115–31.
Liu W, Zhu X, Jing J. The analysis of ductile-brittle failure mode transition in rock cutting. Journal of Petroleum Science and Engineering 2018a;163:311–9.
Liu Q, Jiang Y, Wu Z, Xu X, Liu Q. Investigation of the rock fragmentation process by a single TBM cutter using a Voronoi element-based numerical manifold method. Rock Mechanics and Rock Engineering 2018b;51(4):1137–52.
Lu Z, Wan L, Zeng Q, Zhang X, Gao K. Numerical simulation of fragment separation during rock cutting using a 3D dynamic finite element analysis code. Advances in Materials Science and Engineering 2017. https://doi.org/10.1155/2017/3024918.
Lunow C, Konietzky H. Two dimensional simulation of the pressing and the cutting rock destruction. In: Proceedings of the 2nd international conference on computational methods in tunneling. Aedificatio Publishers; 2009. p. 223–30.
Lv YX, Li HB, Zhu XH, Tang LP. Bonded-cluster simulation of rock-cutting using PFC2D. Cluster Computing 2017;20:1289–301.
Mahabadi OK, Lisjak A, Munjiza A, Grasselli G. Y-Geo: New combined finite-discrete element numerical code for geomechanical applications. International Journal of Geomechanics 2012;12:676–88.
Mendoza Rizo JA. Modeling rock cutting using DEM with crushable particles. MSc Thesis. University of Pittsburgh; 2008.
Mendoza Rizo JA. Considerations for discrete element modeling of rock cutting. PhD Thesis. University of Pittsburgh; 2013.
Menezes PL. Influence of rock mechanical properties and rake angle on the formation of rock fragments during cutting operation. The International Journal of Advanced Manufacturing Technology 2017;90(1–4):127–39.
Menezes PL, Lovell MR, Avdeev IV, Higgs III CF. Studies on the formation of discontinuous rock fragments during cutting operation. International Journal of Rock Mechanics and Mining Sciences 2014;71:131–42.
Miedema SA. The Delft sand, clay and rock cutting model. IOS Press; 2014.
Mohammadnejad M, Liu H, Dehkhoda S, Chan A. Numerical investigation of dynamic rock fragmentation in mechanical cutting using combined FEM/DEM. In: Proceedings of the 3rd nordic rock mechanics Symposium – NRMS 2017. Helsinki: Finland. IRSM; 2017.
Mohammadnejad M, Liu H, Chan A, Dehkhoda S, Fukuda D. An overview on advances in computational fracture mechanics of rock. Geosystem Engineering 2018. https://doi.org/10.1080/12269328.2018.1448006.
Munjiza AA. The combined finite-discrete element method. John Wiley & Sons; 2004.
Munjiza A, John NWM. Mesh size sensitivity of the combined FEM/DEM fracture and fragmentation algorithms. Engineering Fracture Mechanics 2002;69:281–95.
Munjiza A, Andrews KRF, White JK. Combined single and smeared crack model in combined finite-discrete element analysis. International Journal for Numerical Methods in Engineering 1998;44:41–57.
Nakashima S, Sakamoto T, Shimizu N. Effect of element surface roughness on brittle failure in hard rocks by DEM simulation. In: Rock mechanics and rock engineering: from the past to the future. CRC Press; 2016.
Nishimatsu Y. The mechanics of rock cutting. International Journal of Rock Mechanics and Mining Sciences & Geomechanics Abstracts 1972;9(2):261–70.
Richard T. Determination of rock strength from cutting tests. MSc Thesis. University of Minnesota; 1999.
Richard T, Detournay E, Drescher A, Nicodeme P, Fourmaintraux D. The scratch test as a means to measure strength of sedimentary rocks. In: Proceedings of the SPE/ISRM conference on rock mechanics in petroleum engineering. Trondheim, Norway: Society of Petroleum Engineers; 1998.
Richard T, Dagrain F, Poyol E, Detournay E. Rock strength determination from scratch tests. Engineering Geology 2012;147–148:91–100.
Rougier E, Knight E, Lei Z, Munjiza A. Recent development in the combined finite-discrete element method. In: Proceedings of the 1st pan-American congress on

computational mechanics. International Center for Numerical Methods in Engineering (CIMNE); 2015. p. 101–11.
Shao W. A study of rock cutting with point attack picks. PhD Thesis. University of Queensland; 2016.
Solidity. Solidity project.. 2017. http://solidityproject.com.
Song JH, Wang H, Belytschko T. A comparative study on finite element methods for dynamic fracture. Computational Mechanics 2008;42:239–50.
Stavropoulou M. Modeling of small-diameter rotary drilling tests on marbles. International Journal of Rock Mechanics and Mining Sciences 2006;43:1034–51.
Tan X, Kou S, Lindqvist PA. Application of the DDM and fracture mechanics model on the simulation of rock breakage by mechanical tools. Engineering Geology 1998;49:277–84.
Tang CA, Hudson JA. Rock failure mechanisms: illustrated and explained. Taylor & Francis; 2010.
Tatone BSA, Grasselli G. A calibration procedure for two-dimensional laboratory-scale hybrid finite–discrete element simulations. International Journal of Rock Mechanics and Mining Sciences 2015;75:56–72.
Thuro K, Schormair N. Fracture propagation in anisotropic rock during drilling and cutting. Geomechanics and Tunnelling 2008;1:8–17.
Tijssens MGA, Sluys BLJ, van der Giessen E. Numerical simulation of quasi-brittle fracture using damaging cohesive surfaces. European Journal of Mechanics – A/Solids 2000;19:761–79.
Wang S, Sloan S, Liu H, Tang C. Numerical simulation of the rock fragmentation process induced by two drill bits subjected to static and dynamic (impact) loading. Rock Mechanics and Rock Engineering 2011;44:317–32.
Xia YM, Guo B, Cong GQ, Zhang XH, Zeng GY. Numerical simulation of rock fragmentation induced by a single TBM disc cutter close to a side free surface. International Journal of Rock Mechanics and Mining Sciences 2017;91:40–8.
Xiao N, Zhou XP, Gong QM. The modelling of rock breakage process by TBM rolling cutters using 3D FEM-SPH coupled method. Tunnelling and Underground Space Technology 2017;61:90–103.
Yu B. Numerical simulation of continuous miner rock cutting process. PhD Thesis. West Virginia University; 2005.
Zhang ZX. Rock fracture and blasting: theory and applications. Butterworth-Heinemann; 2016.
Zhang QQ, Han ZN, Zhang MQ, Zhang JG. Prediction of tool forces in rock cutting using discrete element method. Electronic Journal of Geotechnical Engineering 2015;20(5):1607–25.
Zhou Y, Lin JS. On the critical failure mode transition depth for rock cutting. International Journal of Rock Mechanics and Mining Sciences 2013;62:131–7.
Zhou Y, Lin JS. Modeling the ductile-brittle failure mode transition in rock cutting. Engineering Fracture Mechanics 2014;127:135–47.
Zhu X, Liu W, He X. The investigation of rock indentation simulation based on discrete element method. KSCE Journal of Civil Engineering 2017;21:1201–12.

**Sevda Dehkhoda** is a senior mining engineer with technical expertise in rock fracture mechanics, fragmentation, and alternative rock breakage methods for hard rock mining. She holds BSc and MSc degrees in Mining Engineering, and PhD in novel rock breakage system for mining. Sevda's career spans over academia, research & development, and technical consulting for mining and civil industries in Australia and the Middle East. Over the last decade, Sevda has led development and testing of several mining related technologies in the areas of continuous hard rock mining, automation and sensing for rock breakage systems. Sevda is currently working with Hatch, a global consulting firm across the mining, energy and infrastructure sectors. Based in Brisbane in Australia, she applies her knowledge in mining technology and innovation, bridging the gap between technology development and widespread application.

**Hongyuan Liu** is currently a senior lecturer at University of Tasmania (UTAS) in Australia and a Fellow of Institute of Engineers Australia. He completed his PhD at Lulea University of Technology in Sweden and masters & bachelor degrees at Northeastern University in China. Before joining in UTAS as a lecturer, he had worked as a research fellow and postdoctoral fellow in University of Queensland and University of Sydney, respectively. He has published over 70 articles in international journals, which leads to an H-index of 28 and 2174 citations. He currently supervises three PhD students and leads a geomechanics research group at UTAS. His research interests include computational geomechanics, mechanical fragmentation, rock blasting, and tunnelling. He is the author of three software for rock mechanics and tunnelling, namely HFDEM, TunGeo3D and RFPA. His paper on the development of HFDEM (hybrid finite-discrete element method) was one of the Highly Ranked Papers in the 12th (2012) ANZ Geomechanics Conference. His team's series of papers on further development and parallelization of HFDEM were selected as the Best Paper Awards of the 3rd (2018) an 4th (2019) Australasian Conference on Computational Mechanics (ACCM) and the only Excellent Paper Award in the 5th (2019) ISRM Young Scholars' Symposium on Rock Mechanics and International Symposium on Rock Engineering for Innovative Future. He hosted a workshop disseminating HFDEM, its parallelisation on the basis of general purpose graphic processing unit and its application in modelling rock fracture and fragmentation during ACCM 2019, where he was the conference co-chair.